A Gaussian Moment-Conservation Diffusion Model[1]

J. D. SHANNON

Atmospheric Physics Section, Radiological and Environmental Research Division, Argonne National Laboratory, Argonne, IL 60439

(Manuscript received 15 August 1978, in final form 25 July 1979)

ABSTRACT

A new method of solution of the advection-diffusion equation is developed; the key feature of the method is the approximate conservation of the zeroth, first and second moments of pollutant mass, with the assumption of Gaussian subgrid-scale distributions. Test cases used in evaluation of other numerical dispersion techniques are simulated with the Gaussian moment-conservation (GMC) model; the tests attempt to quantify numerical error and computation time requirements. The GMC technique is found to be computationally rapid and applicable to telescoping grid systems, and to model diffusion accurately. In a limited number of test cases, the GMC technique exhibits a phase speed lag of about 10%, with considerable pseudodiffusion and dispersion of short waves for the advective case when initial gradients are steep.

1. Introduction

A variety of numerical methods have been proposed for grid models of pollutant dispersion. Common problems frequently critical in simulations are spurious short waves or numerical pseudodiffusion due to the computational scheme, rather than to the physical case being modeled. In some instances numerical errors are so large (Long and Pepper, 1976) that application of a particular numerical method may be unwise. Thus, evaluation of a numerical model of dispersion should address the errors resulting from the numerical techniques employed, as well as the general applicability, data requirements and computational efficiency of the model. In such a manner, this paper describes and examines the Gaussian moment-conservation (GMC) model, which combines concepts involved in the particle-in-cell model of Sklarew *et al.* (1971), the conservation-of-moments model of Egan and Mahoney (1972), and the puff-on-cell model of Sheih (1978).

Any assumption about subgrid-scale distributions in a numerical model is somewhat arbitrary, since typically a single number describes the distribution of pollutant within a grid cell. For instance, Egan and Mahoney (1972) assume rectangular distributions or combinations of rectangular distributions within grid cells, while Sheih (1978) assumes Gaussian distributions. In the GMC model, initial distributions within grid cells (basis puffs) are assumed to be Gaussian, the basis puffs are transported and diffused by the real wind plus an artificial diffusion wind, and the zeroth, first and second moments are conserved (approximately) in redistribution of the basis puffs in order to minimize numerical error.

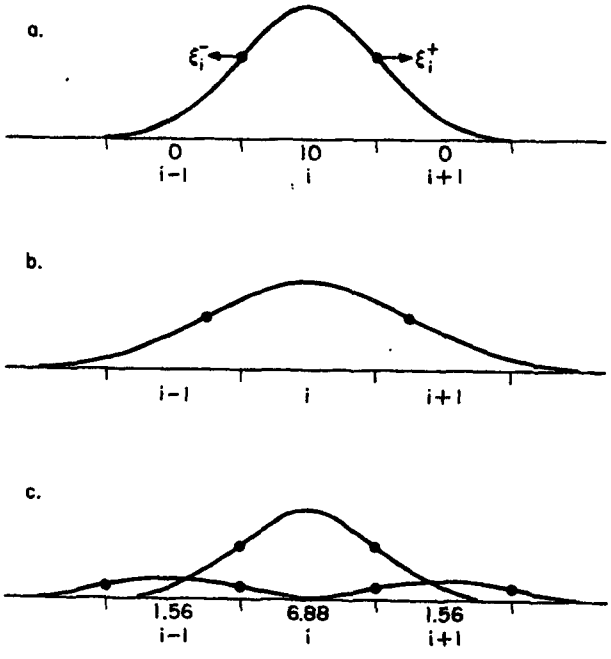

FIG. 1. Schematic of GMC technique for diffusion.

[1] Work performed under the auspices of the U.S. Department of Energy.

0021-8952/79/111406-09$06.25

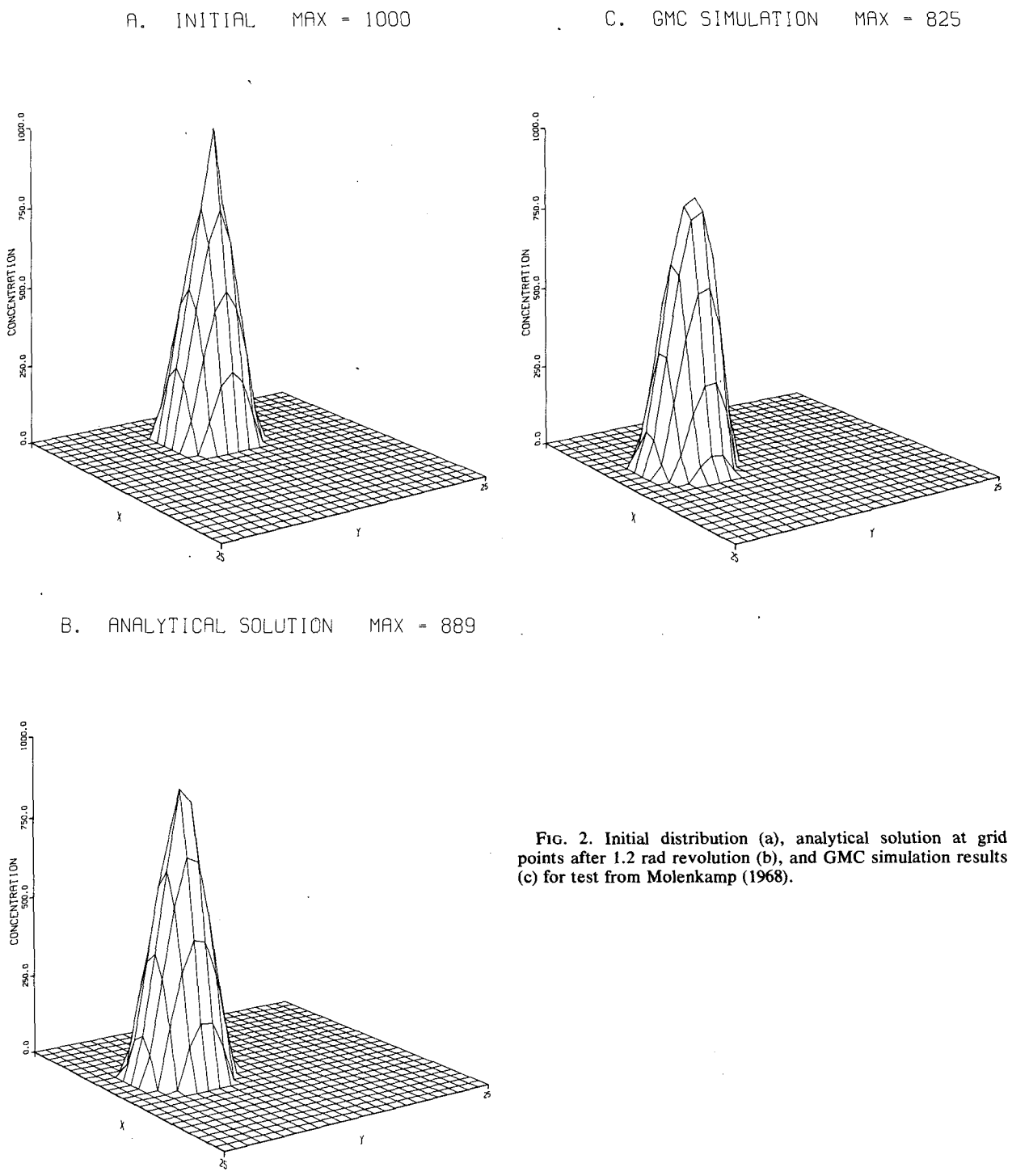

FIG. 2. Initial distribution (a), analytical solution at grid points after 1.2 rad revolution (b), and GMC simulation results (c) for test from Molenkamp (1968).

2. The model

The following development is for the one-dimensional case with nonuniform grid spacing. Extension to two or three dimensions is straightforward; the equations can be simplified for a uniform grid. For a conservative pollutant in an incompressible fluid, the advection-diffusion equation can be written

$$\frac{\partial C}{\partial t} = -u\frac{\partial C}{\partial x} + \frac{\partial}{\partial x}\left(K_x\frac{\partial C}{\partial x}\right), \qquad (1)$$

where C is concentration, x and t are space and time variables, and K_x and u are the appropriate

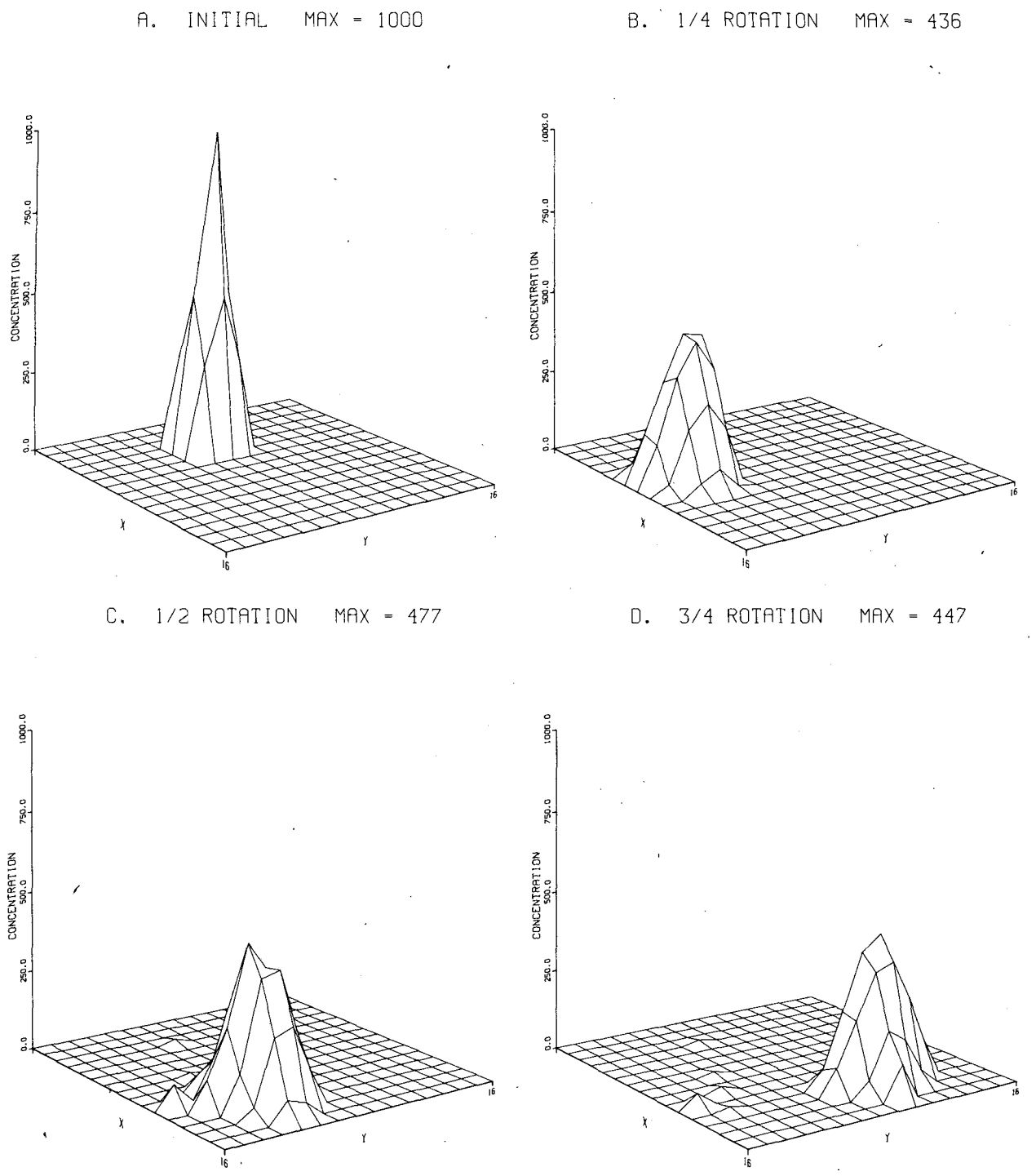

FIG. 3. Initial distribution (a) and GMC simulation results (b)–(e) for test from Christensen and Prahm (1976).

components of eddy diffusivity and wind, respectively. A diagram illustrating the discussion below is shown in Fig. 1. As in Sheih (1978), the initial distribution within cell i is assumed to be Gaussian with a standard deviation σ of one-half of the grid increment, or $\Delta x_i/2$. The concept of Sklarew *et al.* (1971) is followed in defining at each cell boundary a diffusive velocity ξ such that

$$\xi = -\frac{K_x}{C}\frac{\partial C}{\partial x}. \tag{2}$$

The diffusive velocity is an artificial downgradient

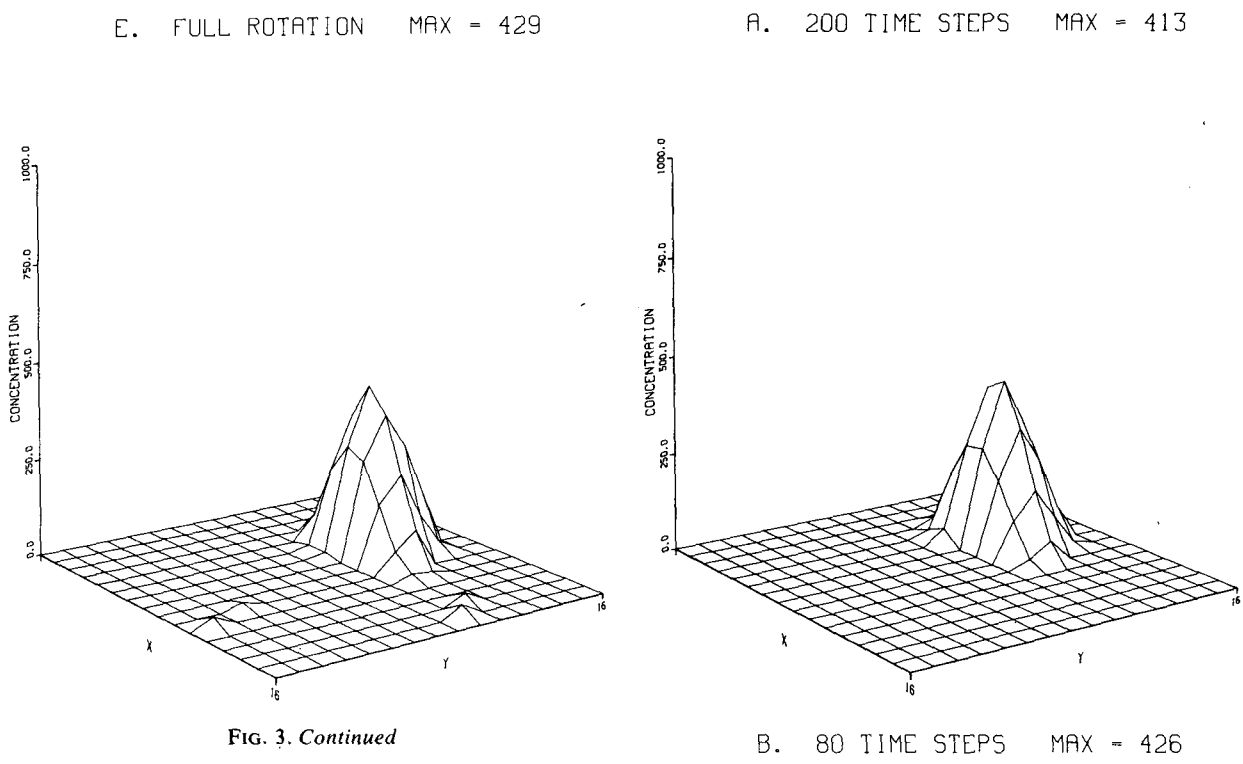

FIG. 3. *Continued*

wind. In their particle-in-cell model, Sklarew *et al.* (1971) calculate their "turbulent flux velocity" at the position of each particle, which represents a known pollutant mass, and transport the particle with the resultant of the turbulent flux velocity and the real wind. In the GMC model, the diffusive velocity is calculated at the boundaries between grid cells, which are the initial ± 1 standard deviation positions of the Gaussian distribution of the basis puffs. After the $\pm\sigma$ positions are shifted by the diffusive velocity and the real wind, the new center of the basis puff is considered to be midway between the new locations of the two points, with σ equal to half of the new distance between the two points. In the version of the GMC model presented here, the real wind is expressed as the average value across a basis puff, and thus the basis puff is stretched only by the diffusive wind. If the real wind varies across the basis puff, then divergence in the real wind also can change the basis puff standard deviation.

Diffusive velocities ξ_i^+ and ξ_i^-, where the superscripts represent the boundaries between cells i and $i+1$ and between i and $i-1$, respectively, are calculated in the examples to follow by centered finite differences. During a time increment Δt, the basis puff in cell i is expanded by the diffusive velocities to

$$\sigma_i = \Delta x_i/2 + (\xi_i^+ - \xi_i^-)\Delta t/2, \tag{3}$$

and shifted by the real and diffusive velocities to

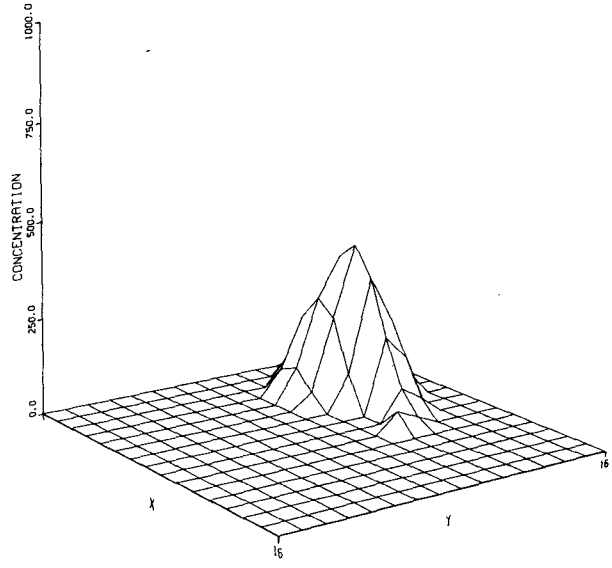

FIG. 4. Effect of increasing time increment in GMC simulation for test from Christensen and Prahm (1976).

$$\mu_i = (u_i + (\xi_i^+ + \xi_i^-)/2)\Delta t, \tag{4}$$

where u_i is the real wind in cell i and $\mu_i = 0$ at the center of cell i.

After a time increment of dispersion, the shifted basis puff initially in cell i is apportioned to new

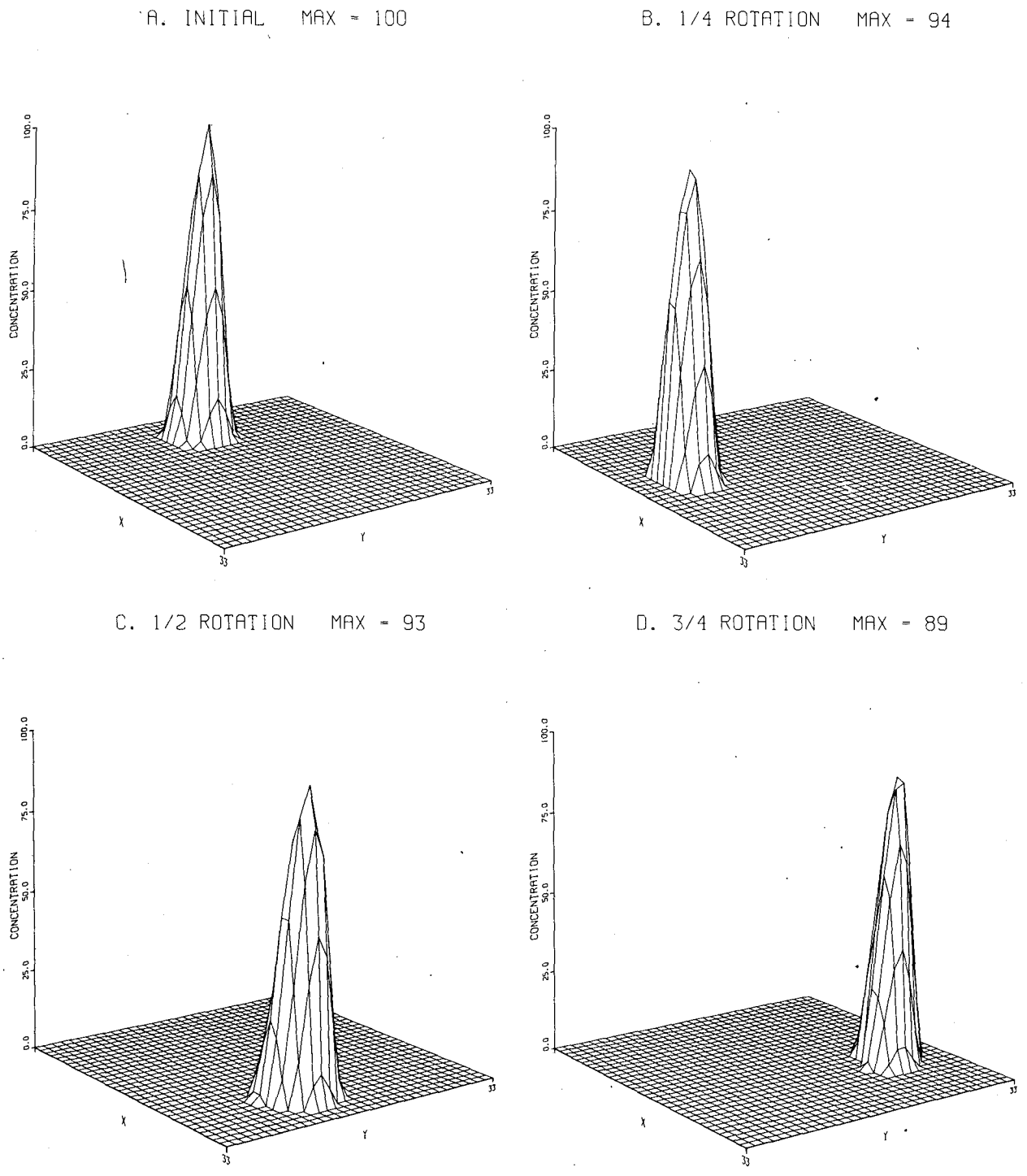

FIG. 5. Initial distribution (a) and GMC simulation results (b)–(e) for test from Long and Pepper (1976).

Gaussian basis puffs in cells $i-1$, i and $i+1$ in a manner such that the zeroth, first and second moments about the center of cell i are conserved. Concentration C_i (per unit length) represents a pollutant mass $C_i\Delta x_i$. After normalization by this mass, the moment equations can be expressed as

$$M_{i,i-1} + M_{i,i} + M_{i,i+1} = 1, \tag{5}$$

$$-M_{i,i-1}\left(\frac{\Delta x_{i-1} + \Delta x_i}{2}\right) + M_{i,i+1}\left(\frac{\Delta x_i + \Delta x_{i+1}}{2}\right) = \mu_i, \tag{6}$$

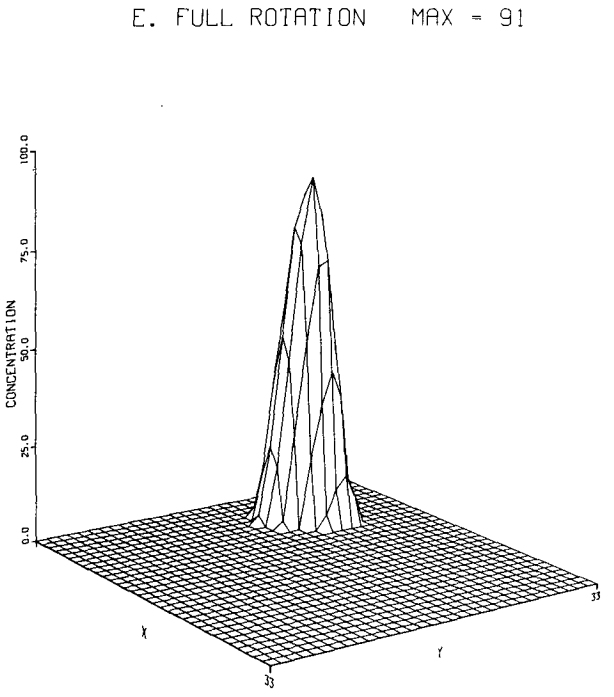

FIG. 5. *Continued*

$$M_{i,i-1}\left[\left(\frac{\Delta x_{i-1}}{2}\right)^2 + \left(\frac{\Delta x_{i-1} + \Delta x_i}{2}\right)^2\right] + M_{i,i}\left(\frac{\Delta x_i}{2}\right)^2 + M_{i,i+1}\left[\left(\frac{\Delta x_{i+1}}{2}\right)^2 + \left(\frac{\Delta x_i + \Delta x_{i+1}}{2}\right)^2\right] = \sigma_i^2 + \mu_i^2, \quad (7)$$

where $M_{i,i-1}$, $M_{i,i}$ and $M_{i,i+1}$ represent the portion of the mass, originally within cell i, within cells $i-1, i$ and $i+1$, respectively, after allocation. Eq. (5) conserves mass. Eq. (6) states that the center of mass of the three basis puffs is equal to the center of mass of the single basis puff after dispersion. Eq. (7) sets the within-puff and between-puff second moments of the three basis puffs equal to the second moment of the single basis puff after dispersion. Eqs. (5), (6) and (7) can be solved for $M_{i,i-1}$, $M_{i,i}$ and $M_{i,i+1}$. After dispersion of the initial basis puffs within each cell has taken place, the pollutant mass in the ith cell is

$$C_i^{j+1}\Delta x_i = C_{i-1}^j \Delta x_{i-1} M_{i-1,i} + C_i^j \Delta x_i M_{i,i} + C_{i+1}^j \Delta x_{i+1} M_{i+1,i}, \quad (8)$$

where superscripts j and $j+1$ denote time steps. It is possible, or even probable, that some of the M values will be negative. Negative mass and negative concentration have no physical meaning. For the grid system as a whole, after dispersion has taken place for all cells, most negative mass is counterbalanced by positive mass dispersed from other cells. All grid cells containing a net negative mass are set to zero after summation of the negative masses; net positive masses in the other cells are scaled by a factor equal to $(\Sigma\text{pos} + \Sigma\text{neg})/\Sigma\text{pos}$. This adjustment conserves mass, but the first and second moments are no longer conserved exactly.

When dispersion is modeled in two or three dimensions, (5)–(7) are solved for each dimension, and the mass allotments are obtained by the appropriate products of fractions.

The treatment of grid boundaries can be quite simple. In the examples in the next section, the diffusive velocity on the outer side of each perimeter cell is assumed to be the same as that on the inner side. This simple assumption is effective as long as the concentration gradient at the boundary is inward; a different assumption would be necessary for upwind sources outside the computation grid. In a one-dimensional version of the model used for pollutant budget calculations (Shannon, 1979), the top of the grid and the ground are absolute barriers to diffusion ($K_z = 0$), although removal at the surface is simulated by the customary method involving deposition velocity.

3. Evaluation of the GMC technique

Several authors have examined the accuracy of numerical schemes for solving the advection-diffusion equation [e.g., Molenkamp (1968), Christensen and Prahm (1976), Long and Pepper (1976) and Pepper and Long (1978); hereafter referred to as M, CP, LP and PL, respectively]. One of the common tests is pure rotation of a conical or similar symmetric distribution in a field of uniform

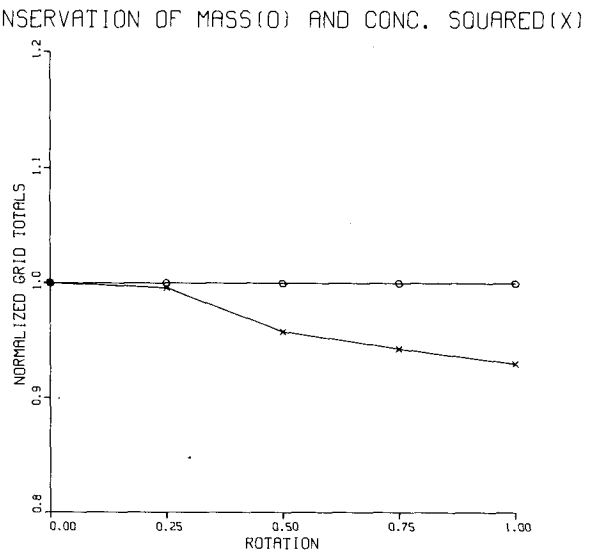

FIG. 6. Conservation of mass and cell concentration squared for GMC simulation for test from Long and Pepper (1976).

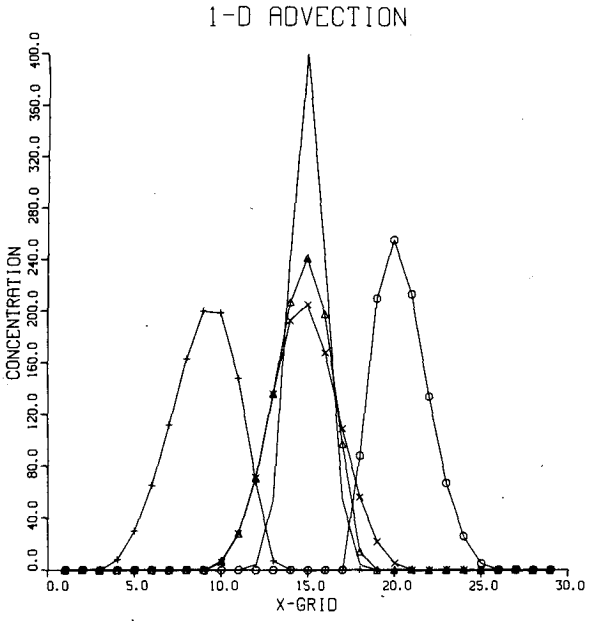

FIG. 7. GMC simulation of cyclic advection in one dimension: $\Delta x = 100$ m, $\Delta t = 120$ s, and $|u| = 0.167$ m s^{-1}. The curve without symbols is the initial distribution; results are shown for 1 (○), 2 (△), 3 (+) and 4 (×) simulation hours. The analytical solutions would be the initial peak centered above each GMC simulation result.

angular velocity. While this does not represent a likely application (real wind fields are never so regular nor so completely described), it does allow examination of numerical error, since a complete rotation without modeled diffusion leaves the analytical solution unchanged; any departure from the original distribution represents pseudo-diffusion or dispersion of spurious short waves.

The test in M involves rotation on a 25 × 25 grid of a conical initial distribution described by

$$C(x,y) = \begin{cases} 1000(1 - r/4\Delta), & r < 4\Delta \\ 0, & r \geq 4\Delta, \end{cases} \quad (9)$$

where $r = [(x - x'')^2 + (y - y'')^2]^{1/2}$, Δ is the grid interval, and $(x'',y'')_0 = (7,13)$ is the initial center of the cone, located away from the boundaries and the axis of rotation. The angular velocity is -0.001 rad s^{-1}, the time increment is 30 s, and evaluation is made after 40 time steps, or 1.2 rad rotation. The initial distribution and the analytical solution at grid points after the rotation are shown in Figs. 2a and 2b. The apparent decrease of the maximum and loss of symmetry result from the partial rotation not centering the analytical solution on a grid cell. For a similar test performed with the GMC technique (Fig. 2c), the maximum concentration after the partial rotation is 83% of the original maximum or 93% of the analytical maximum at a grid cell center after partial rotation. The minimum value with the GMC technique is zero, as in the analytical solution, since the GMC technique contains an algorithm to eliminate negative values. The GMC solution has also lagged slightly behind the analytical solution.

A similar test in CP is more rigorous, in that the radius of the cone is two grid increments rather than four and the gradient is thus much steeper. The cone is rotated on a 12 × 12 grid, or 16 × 16 after allowance for a boundary "sponge." The test is for a full rotation; thus the initial distribution (Fig. 3a) is also the analytical solution after rotation. When the same test is applied to the GMC technique, numerical error disperses the concentration considerably, as shown in the sequence of Figs. 3b–3e. The lag in rotation of the maximum (~15% in this case) can be noted. The GMC test in Fig. 3 uses 800 time steps for the complete rotation as in CP. For GMC rotations in 200 and 80 time steps, the respective final results are shown in Figs. 4a and 4b. A comparison with Fig. 3e indicates that the GMC results are little changed over a tenfold increase in the time increment.

The tests by LP and PL involve rotation on a 33 × 33 grid of a cosine "hill" described by

$$C_{i,j} = \begin{cases} [1 + \cos(\pi R/4)]50, & R \leq 4, \quad (10) \\ 0, & R > 4, \quad (11) \end{cases}$$

$$R^2 = (x_i - x_0)^2 + (y_i - y_0)^2, \quad (12)$$

$$(x_0,y_0) = (7,17). \quad (13)$$

With this and similar tests, LP and PL examine the

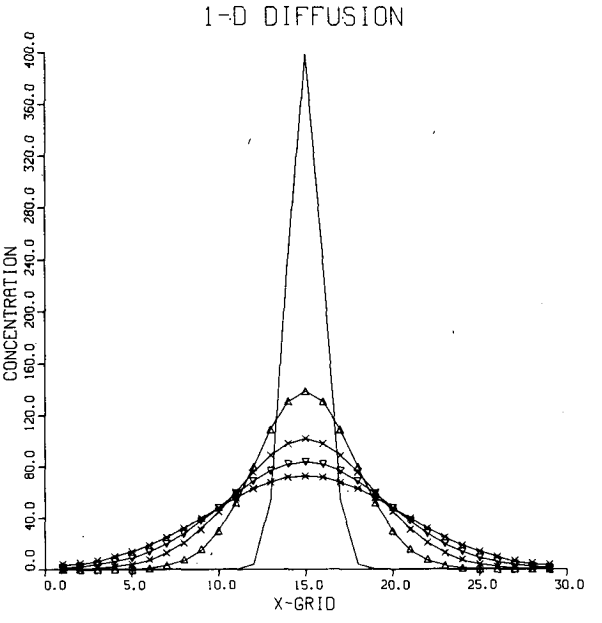

FIG. 8. GMC simulation of diffusion in one dimension: $\Delta x = 100$ m, $\Delta t = 120$ s, and $K_x = 10$ m^2 s^{-1}. The spike is the initial distribution; other curves are analytical solutions after 1 (△), 2 (×), 3 (▽), and 4 (*) simulation hours; symbols are corresponding GMC results.

changes with rotation of the hill shape, conservation of mass, and conservation of the sum of squares of cell concentrations for various techniques. Results from a test of the GMC technique are shown in Figs. 5a–5e and 6. Phase speed and the peak concentration after rotation are each reduced ~10%. Mass is conserved but the sum of squares of concentrations decreases ~10%. The full rotation (240 time steps) required 4s of CPU time on an IBM 370/195.

Some tests of pure cyclic advection, pure diffusion, advection plus diffusion, sensitivity to the time increment and variable grid spacing have been made in one dimension for ease in analysis. As might be expected from the two-dimensional simulations, the simulation of pure advection (Fig. 7) dispersed considerably, particularly during the first stages when gradients are steepest. Pure diffusion (Fig. 8) is predicted quite accurately; an advection-plus-diffusion simulation (Fig. 9) is almost as accurate. When the diffusion simulations are varied over a range of time increments between 60 and 360 s, results are almost unchanged (Fig. 10). A telescoping grid is examined for pure diffusion (Fig. 11); the grid lengths vary from 50 to 200 m. The differences from the predictions with a regular grid are minor.

A possible source of numerical error when diffusion is simulated is the finite-difference approximation for the concentration gradient. This error could no doubt be reduced by a cubic spline or other improved mathematical approximation, although at some cost in speed of computation, but the results above indicate that the refinement is unnecessary. The more significant source of error, in the advective case, is the algorithm by which negative values are eliminated. The technique modifies the first and second moments, and thus

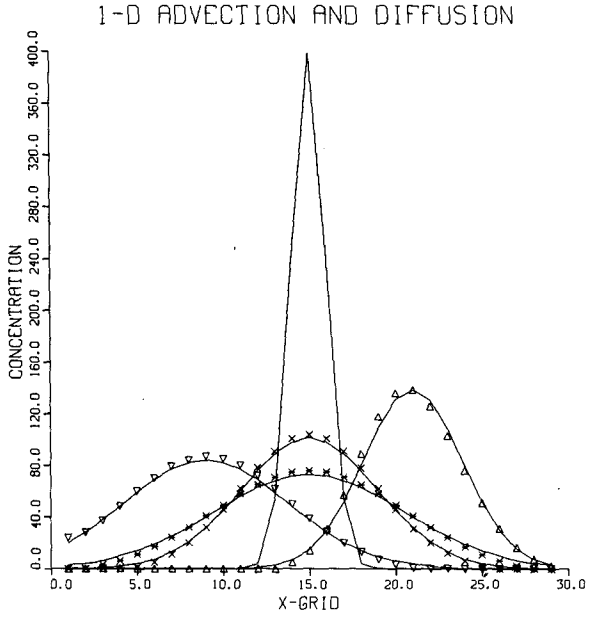

FIG. 9. GMC simulation of cyclic advection plus diffusion in one dimension: Δx = 100 m, Δt = 120 s, K_x = 10 m^2 s^{-1} and $|u|$ = 0.167 m s^{-1}. Curves are the initial distribution and analytical solutions after 1 (△), 2 (×), 3 (▽), and 4 (*) hours; symbols are corresponding GMC results.

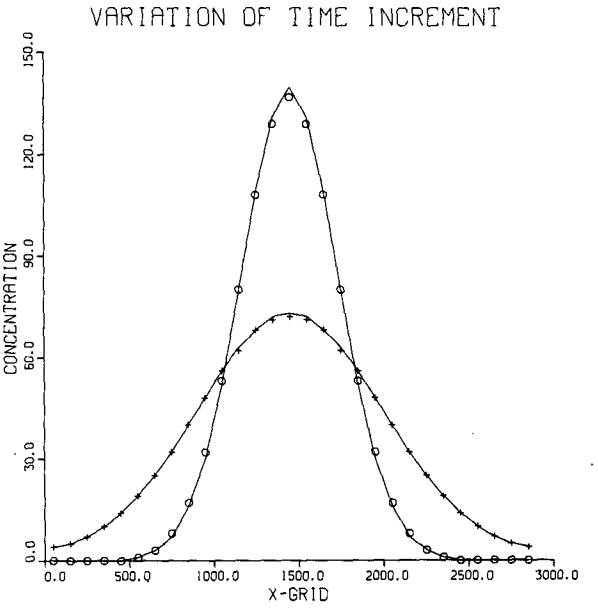

FIG. 10. GMC simulation of pure diffusion for 1 and 4 h of diffusion for Δt = 60 s (curves) and Δt = 360 s (symbols); Δx = 100 m and K_x = 10 m^2 s^{-1}.

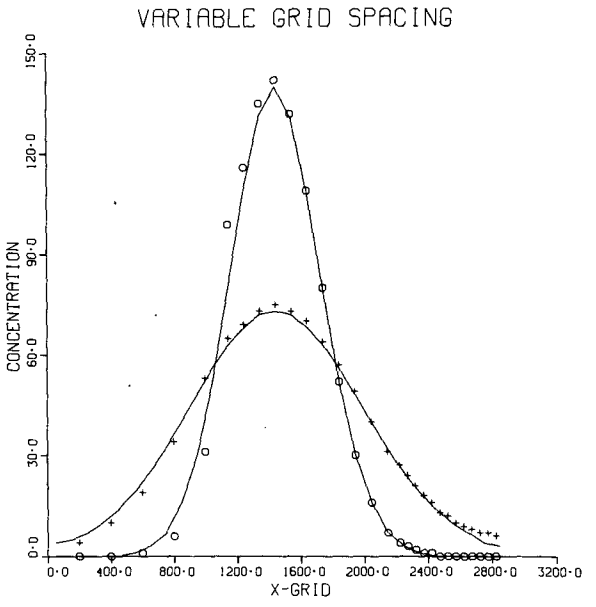

FIG. 11. GMC simulation of 1 and 4 h of pure diffusion with a uniform grid (curves; Δx = 100 m) and a telescoping grid [symbols; Δx = 5(200 m) + 11(100 m) + 13(50 m)]; Δt = 60 s and K_x = 10 m^2 s^{-1}.

gradually changes the distribution. Other algorithms have been tried, such as eliminating negative mass only after a given number of time steps; pseudo-diffusion is somewhat decreased but the rotational lag is increased.

It is extremely difficult to compare computation times with simulations in other studies, since differences in computer capabilities and programming efficiency may mask the actual differences in computation requirements. However, a rough evaluation can be made of the speed of the GMC technique from a particular application. The GMC technique has been used in the vertical budget subprogram of a long-term regional sulfur pollution model (Shannon, 1979). The program involves separate calculations of releases from three different release heights at eight times during the day for a three-day simulation involving two pollutants. The $3 \times 8 \times 3 \times 2 = 144$ days total integration of the 20-layer model (minimum grid interval is 25 m; maximum eddy diffusivity for the corresponding layer is 10 $m^2 s^{-1}$) requires ~250 s CPU time, including output, on the IBM 370/195 at Argonne National Laboratory.

4. Conclusion

The Gaussian moment-conservation technique for numerical solution of the advection-diffusion equation has been shown to be computationally rapid, to model diffusion accurately, but to experience significant numerical error for the advective case when gradients are steep. The likely cause of the latter numerical error is the adjustment of the exact solution of the Gaussian moment equations in order to avoid negative concentrations. The most promising application of the GMC technique in its present development appears to be modeling of pure diffusion in situations in which repeated simulations, such as for sensitivity testing or examination of alternate scenarios, require computational efficiency. The model could also be used for prediction of advection if the initial field is relatively smooth.

Acknowledgment. This work is supported by the U.S. Department of Energy and the Environmental Protection Agency. The reviewing efforts of C. M. Sheih, M. L. Wesely and P. E. Long are most appreciated.

REFERENCES

Christensen, O., and L. P. Prahm, 1976: A pseudospectral model for dispersion of atmospheric pollutants. *J. Appl. Meteor.*, **15**, 1284–1294.

Egan, B. A., and J. R. Mahoney, 1972: Numerical modeling of advection and diffusion of urban area source pollutants. *J. Appl. Meteor.*, **11**, 312–322.

Long, P. E., and D. W. Pepper, 1976: A comparison of six numerical schemes for calculating the advection of atmospheric pollution. *Preprints Third Symp. Atmospheric Turbulence, Diffusion and Air Quality*, Raleigh, Amer. Meteor. Soc., 181–187.

Molenkamp, C. R., 1968: Accuracy of finite-difference methods applied to the advection equation. *J. Appl. Meteor.*, **7**, 160–167.

Pepper, D. W., and P. E. Long, 1978: A comparison of results using second-moments with and without width corrections to solve the advection equation. *J. Appl. Meteor.*, **17**, 228–233.

Shannon, J. D., 1979: The Advanced Statistical Trajectory Regional Air Pollution Model. Radiological and Environmental Research Division, Argonne National Laboratory, Topical Report ANL/RER-79-1, 33 pp.

Sheih, C. M., 1978:: A puff-on-cell model for computing pollutant transport and diffusion. *J. Appl. Meteor.*, **17**, 140–147.

Sklarew, R. C., A. J. Fabrick and J. E. Prager, 1971: A particle-in-cell method for numerical solution of the atmospheric diffusion equation, and applications to air pollution problems. Division of Meteorology, National Environmental Research Center, Rep. 35R-844, 150 pp.